Chapter 9

Fundamental Role of Periodicity and Geometric Shape to Resonant Terahertz Transmission

Joong Wook Lee and DaiSik Kim

Additional information is available at the end of the chapter

http://dx.doi.org/10.5772/48243

1. Introduction

Optical properties of the plasmonic structures based on the surface of variously structured metal plates became a subject of intense research ever since Ebbesen et al. reported the enhanced optical transmission through subwavelength hole arrays [1]. Their experimental results provided evidence that the enhanced optical properties originate from the coupling between the incident light and surface plasmon modes. Studies of such plasmonic structures and its mechanisms have a long history in the development of electromagnetism, though it has been an intense subject of research in recent years.

In the 1900s, Wood and Rayleigh reported the anomalous optical properties of reflection gratings [2,3], which are intimately connected with the excitation of surface bound waves on the metal-dielectric interfaces [4]. Hessel and Oliner presented two types of the anomalies occurring in the reflection grating surface: a Rayleigh wavelength type attributed to the usual propagating surface plasmon modes and a resonance type which is related to the guided waves supported by the grating itself [5]. On the other hand, since the 1970s, the optical properties of transmission gratings or grids have been occasionally studied in the microwave, terahertz (THz), and infrared regions [6-10]. In particular, Lochbihler and Depine in 1993 presented a theoretical approach for calculating the fields diffracted by the gratings made of highly conducting wires [11]. Here they calculated Maxwell's equations based on modal expansions inside the metal and Rayleigh expansions outside the metal, applying the theoretical treatments by means of surface impedance boundary condition method [11,12].

This research field reinvigorated after the Ebbesen's pioneering work which was focused on the understanding of mechanisms of the enhanced transmission through periodically perforated holes or slits on metallic plates. The one-dimensional plasmonic structures with periodic arrays of slits have been studied by some groups with theoretical and experimental

approaches in the optical region [13-18]. These results strongly support the existence of two mechanisms of generating enhanced optical transmission: the geometric shape controlled mainly by the slit thickness and the periodicity determining the excitation of coupled surface plasmon polaritons (SPPs) on both surfaces of the perforated metallic structures. In particular the former called as a Fabry-Perot-like behavior was studied theoretically in a single narrow slit and clearly verified by strong resonant transmission of microwave radiation [19,20].

On the other hand in two-dimensional plasmonic structures with periodic arrays of holes, the geometric shape effect has been underestimated in spite of many researches about the strong transmission enhancement in the optical region [21-26]. Recently, the geometric shape resonance however was emerged as one of the dominant mechanisms of the strong transmission enhancement [27-29]. In particular, Koerkamp et al. already noted that the strong optical transmission is strongly influenced by a hole shape and a shape change from circular to rectangular [30]. The importance of the geometric shape was also confirmed by studies of strong enhancement of the light transmission through random arrays of holes [30-32] and single apertures [33-36], in particular a single rectangular hole theoretically studied by Garcia-Vidal et al. [37].

Unlike most typical systems in optical and infrared regions, THz time-domain spectroscopy system based on coherent THz radiation is ideally suited for phase-sensitive, broadband transmission measurements [38-41]. Furthermore, long wavelengths in THz region, 3000 μm to 30 μm (0.1 THz to 10 THz) in general, permit relatively simple fabrication of free-standing samples which can exclude complex surface modes by the substrate. For these reasons, the coherent THz waves have been generally used to study SPP behaviors [42-55]. The SPPs in the strictest sense however do not exist on perfectly conducting metal-dielectric interfaces since surface electromagnetic fields on the dielectric side cannot be strongly confined to the interface. However, recently the concept of the SPP has been extended even to include perfectly good metals with corrugations, which is referred to simply as designer (or spoof) SPP [56-58]. Pendry et al. reported the electromagnetic surface excitations localized near the surface which are governed by an effective permittivity of the same plasma form [56].

In the THz region, the most important thing is that the perfect transmission, of up to near-unity, at specific frequencies can be achieved since most metals become perfect conductor and therefore have extremely small ohmic loss fraction. Until now, a few groups have theoretically predicted the perfect transmission [59-64] and experimentally observed the near-unity transmission [65-67] in the plasmonic structures with periodic arrays of slits and holes. However, despite great progresses in realizing the perfect transmission, we do not have the clear understanding of what are the relative contributions of the geometric shape and the periodicity effects toward the perfect transmission in specific conditions.

Here, we first report on the importance of the combined effects of the geometric shape and periodicity in enhancing THz transmission through one-dimensional periodic arrays of slits. Theoretical predictions based on perfect conductor model show that the measured transmission peaks lie within the broad geometric shape band. We also report that the

perfect transmission can be realized by the geometric shape resonance appearing in spectral region below first Rayleigh minimum. Calculated near-field distributions confirm that the perfect transmission is caused by the concentration of the electric and magnetic fields within the silts. Furthermore, we find that, despite the existence of only the geometric shape effect in random arrays of slits of relatively thick thicknesses, the enhanced transmission comes to the perfect transmission in the long wavelength region. Angle dependent transmission spectra and relative phase measurements clarify the relative roles of the geometric shape and periodicity toward the perfect transmission.

2. Experimental setup

In our experiments, we used a standard THz time-domain spectroscopy system with a spectral range from 0.1 to 2.5 THz, based on a femtosecond Ti:sapphire laser which generates optical pulses with average power of 600 mW and temporal width of about 120 fs set at a center wavelength of 760 nm. Experimental setup is shown in Fig. 1. A photoconducting antenna method is used to generate THz pulses. A crystal for the emitter is undoped, <110> orientated semi-insulating GaAs (INGCRYS Laser System Ltd.) with dark resistivity in range 5.3×10^7 to 5.6×10^7 Ohm cm. Two metallic electrodes are painted by silver paint on one side of the crystal, having a separation of about 0.4 mm which is among a large aperture emitter. Unlike a typical biased system of the photoconductive antenna, an ac bias voltage of 300 V and 50 kHz square wave was applied to the electrodes of the crystal [68]. To make this system, we used a high voltage pulse generator (DEI Model PVX-4150) which generates the squared high-voltage sources by combining DC high voltage source from a power supply (F. u. G. Model MCL 140-650) with square function generated using a pulse/function generator.

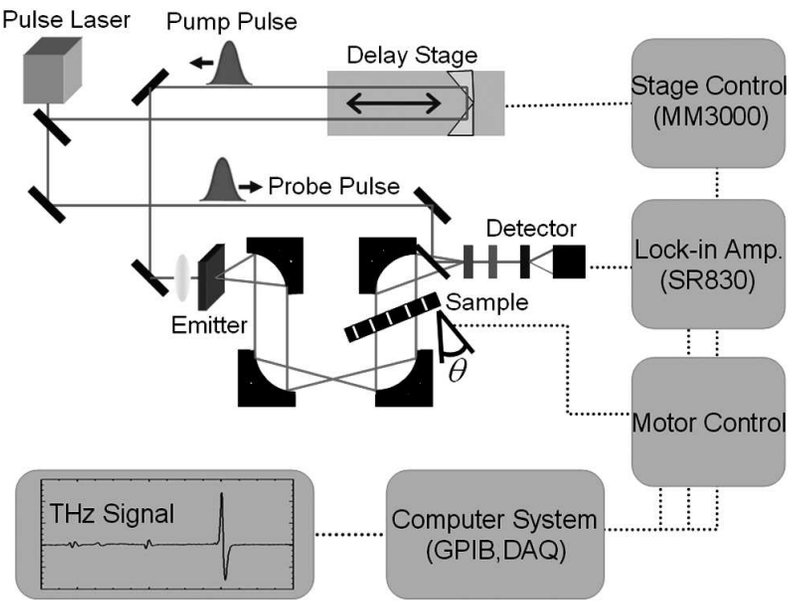

Figure 1. Schematic diagram of the THz time-domain spectroscopy setup. The angle dependent transmission spectra are measured by tilting the sample stage.

Optical pulses generated from the femtosecond Ti:sapphire laser are divided into two parts, pump and probe beams, by a beamsplitter. The pump beam is focused on the surface of the emitter by using a 25 mm focal lens and immediately generates the THz wave which is essentially single cycle electromagnetic pulses. The generated THz wave is collimated by using an off-axis parabolic mirror at a focal distance. The degree of collimation is of the order of $\Delta\theta \sim \lambda/D \sim 1/100$ radian because our beam size D is about 5 cm and the THz wave is a point-like source. The collimated THz wave with the beam diameter of about 5 cm impinges on a reference box or samples. The angle-dependent transmission spectra are measured by tilting the sample stage in range -10 to 50 degrees. The THz pulses transmitted through the samples meet the optical probe beam again on an electro-optic crystal (ZnTe). The polarization change of the optical probe beam due to the Pockels effect is detected by a home-built differential photo-detector and provides us information of both amplitude and phase of the THz wave [69,70]. The signals are automatically acquired by a synchronized system (as shown in Fig. 1) of three components, a motion controller which tilts the sample stage, a data acquisition system, and a delay stage which controls time delay between pump and probe optical pulses. The whole setup is also enclosed in a box which is purged with dry nitrogen gas to reduce the absorption effects of water vapor.

We performed our experiments as follows. First, the collimated THz wave impinges on a reference box made of a 2 cm by 2 cm square hole punctured on a piece of aluminum. We measure the transmission spectrum through the reference box. We then mount our samples with the plasmonic structures of periodic or random arrays of slits perforated on aluminum plates, right on top of the reference box, and measure the transmission spectrum. Our system provides the time-resolved trace of the transmitted THz electric field with subpicosecond temporal resolution as an original signal. The fast Fourier transforms of the measured time-domain THz pulses give us information on both spectral amplitude and phase. The normalization is carried out over the entire frequency simply by dividing the spectral amplitude of the transmitted THz pulse with one of the reference beam transmitting through the reference box.

3. Sample fabrication

The samples were fabricated by a micro-drilling and a femtosecond laser machining methods. The latter is based on laser ablation which is performed by amplified femtosecond pulses. The pulses have energy of up to 1 mJ centered at 800 nm and a repetition rate of 1 kHz. The positions of the focused laser pulses are accurately controlled by using a galvanometer scanner (Scanlab AG, Germany) and a mechanical shutter system. The line edge roughness of the perforated slits is controlled to make successful slit structures, having the LER 3σ value of less than 3 μm which is two orders of magnitude less than the THz wavelengths of interest. The achieved high quality originates from the superiority of femtosecond laser machining system. The samples manufactured by this method have a fixed period d of 500 μm and different thicknesses h of 17, 50, 75 and 153 μm respectively. The silt widths a of these samples are 78, 80, 85, and 83 μm respectively, which are properly designed to be subwavelength [as shown in Fig. 2(a)].

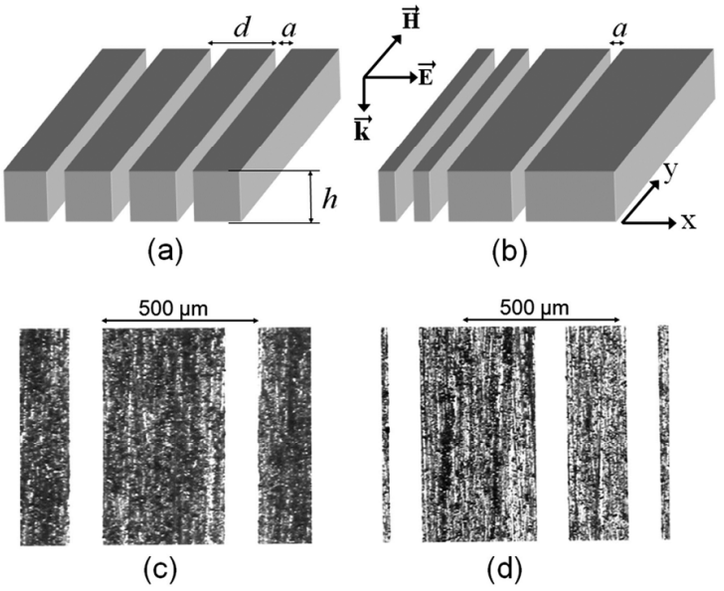

Figure 2. (a), (b) Schematics of the periodic and random arrays of slits of width a, period d, and thickness h, respectively. (c), (d) Microscopic images of the periodic and random arrays of 400 μm thick slits, respectively (Fig. (1) in reference [71]).

On the other hand, the samples with thicknesses of 200 and 400 μm were fabricated by the micro-drilling method by using a screw with a diameter of 100 μm which is a minimum size in diameter of available and commercial screw. These thick plates were chosen for explicitly observing Fabry-Perot-like modes inside the slits. In particular the samples with thickness of 400 μm were considered suitable for randomization of the slit structures, based on the different frozen-phonon fashion of neighboring silts [as shown in Fig. 2(b)]. The position of the *i*th slit by the frozen-phonon fashion is given by

$$x_i = x_0 + id + \Delta x_i \tag{1}$$

where x_0 is the position of the basis of coordinate and Δx_i is the random amount of the *i*th slit which is getting by generating random values [72]. We displaced the position of each slit with random amounts of ± *d*/*4* and ± *d*/*2* which, in this chapter, are called as *Random Type I* and *Random Type II*.

Comparison between transmission properties through random and periodic arrays of slits reveal that the transmission spectra strongly affected by the geometric shape show similar spectral waveforms in both random and periodic arrays, since the geometric shape resonance depends on intrinsic properties of the structure factors not the structural arrangement of the slits. The geometric shape in the one-dimensional plasmonic structures is determined by the thickness h of the slits, providing the Fabry-Perot-like modes $f_c = nc/2h$ where c is the speed of the light in vacuum and n is the integer mode index. In contrast, the periodicity effect might be found in transmission spectra through the periodic arrays not random, having different constructive interference patterns and different far-field transmissions. Therefore the relative contribution of the geometric shape and periodicity is directly compared in this chapter.

4. Theoretical framework

Herein, we are first interested in theoretical approach of THz electromagnetic wave transmission through the periodic arrays of slits, which may allow us to improve our intuitive understanding of the underlying physics and to find the mechanisms enhancing the transmission. To calculate the transmittance, the metallic structures are considered as a perfect conductor so that finite conductivity effects are neglected. This is a good approximation in the THz region, since the real and imaginary parts of dielectric constant of most metals are of the order of -30000 and 100000 respectively. We also consider a simple model system with rectangular shaped slits as shown in Fig. 2(a). In this system, the slits are along the y axis and a direction of propagation of the incident THz wave is the z axis which is normal to the sample surface. The polarization of the incident plane wave is placed along the x axis (TM polarization). Here, there are three different regions: the incident and reflection region (region I), the metal and perforated slit region (region II), and the transmission region (region III).

Let $f(x,z)$ be the spatial function of the component along the z axis of the magnetic field. The fields can be expressed in terms of Rayleigh expansions in region I and III and modal expansion in region II [11,46]. The boundary matching is only carried out at the metal-dielectric interfaces of I-II and II-III since which are semi-infinite. Here we use the single mode approximation inside the slits since the slit width is much smaller than the wavelength. The magnetic fields are described as

$$f_1(x,z) = \sum_{-\infty}^{\infty} (R_n e^{i\chi_n (z+h/2)} + \delta_{n0} e^{-ik(z+h/2)}) e^{i\alpha_x x}, \text{ region I} \tag{2}$$

$$f_3(x,z) = \sum_{-\infty}^{\infty} T_n e^{-i\chi_n (z-h/2)} e^{i\alpha_x x}, \text{ region III} \tag{3}$$

and

$$f_2(z) = A\frac{\sin(kz)}{\sin(kh/2)} + B\frac{\cos(kz)}{\cos(kh/2)}, \text{ region II} \tag{4}$$

where $\alpha_n = 2\pi n/d$, $\chi_n = \sqrt{k^2 - \alpha_n^2}$, $k = \omega/c = 2\pi/\lambda$, and R_n and T_n are the complex amplitudes of the reflected and transmitted diffracted waves respectively. The continuity of the tangential components of the fields implies the continuity of $f(x,z)$ and its normal derivative at $z = \pm h/2$ along $0 \le x \le a$. These conditions are

$$A + B = \sum_{n=-\infty}^{\infty} (R_n + \delta_{n0}) e^{i\alpha_n x} \tag{5}$$

for the continuity of the field at $z = -h/2$,

$$Ak\cot(\frac{kh}{2}) - Bk\tan(\frac{kh}{2}) = \sum_{n=-\infty}^{\infty} (i\chi_n R_n - ik\delta_{n0}) e^{i\alpha_n x} \tag{6}$$

for the continuity of the normal derivative of the field at $z = -h/2$,

$$-A + B = \sum_{n=-\infty}^{\infty} T_n e^{i\alpha_n x} \tag{7}$$

for the continuity of the field at $z = h/2$, and

$$Ak\cot(\frac{kh}{2}) + Bk\tan(\frac{kh}{2}) = \sum_{n=-\infty}^{\infty} (-i\chi_n T_n) e^{i\alpha_n x} \tag{8}$$

for the continuity of the normal derivative of the field at $z = h/2$.

With the orthogonality, we apply some of integral equation to obtain simple solution with proper projection and integration. Multiplying a term $e^{-i\alpha_m x}$ and integrating its results of Eqs. (5)-(8) give

$$A + B = \sum_{n=-\infty}^{\infty} (R_n + \delta_{n0}) P_n \tag{9}$$

$$\left[Ak\cot(\frac{kh}{2}) - Bk\tan(\frac{kh}{2}) \right] Q_n = i\chi_n R_n - ik\delta_{n0} \tag{10}$$

$$-A + B = \sum_{n=-\infty}^{\infty} T_n P_n \tag{11}$$

and

$$\left[Ak\cot(\frac{kh}{2}) + Bk\tan(\frac{kh}{2}) \right] Q_n = -i\chi_n T_n \tag{12}$$

where the quantities P_n and Q_n appearing in Eqs. (9)-(12) are defined as

$$P_n = \frac{1}{a}\int_0^a e^{i\alpha_n x} dx \tag{13}$$

and

$$Q_n = \frac{1}{d}\int_0^a e^{-i\alpha_n x} dx \tag{14}$$

respectively. By using Eqs. (9)-(12) , we obtain

$$A = \frac{P_0}{1 + ikW\cot(kh/2)} \tag{15}$$

$$B = \frac{P_0}{1 - ikW\tan(kh/2)} \tag{16}$$

$$R_n = 1 - \frac{2ikQ_nP_0}{\chi_n}\left[\frac{\cot(kh) - ikW}{1 + k^2W^2 + 2ikW\cot(kh)}\right] \tag{17}$$

and

$$T_n = \frac{2ikQ_nP_0}{\chi_n \sin(kh)}\left[\frac{1}{1 + k^2W^2 + 2ikW\cot(kh)}\right] \tag{18}$$

where W is defined as

$$W = \sum_{n=-\infty}^{\infty} \frac{P_nQ_n}{\chi_n} \tag{19}$$

For normal incidence, zero-order transmittance for the periodic arrays of slits is expressed as follows

$$T_0 = \frac{2ia}{d\sin(kh)}\left[\frac{1}{1 + k^2W^2 + 2ikW\cot(kh)}\right] \tag{20}$$

5. Experimental results

5.1. Enhanced transmission in thin metal plates

Theoretical calculations are first compared with experimental results of samples with the thicknesses of 17, 75 and 153 μm, which are carefully chosen so that the peak positions due to the geometric shape resonance are placed on the higher spectral region than the first Rayleigh minimum. Measured THz time traces and corresponding spectral amplitudes obtained by the fast Fourier transform method are shown in Fig. 3(a) and 3(b) respectively. The top curves in Fig. 3(a) and 3(b) show the reference signals transmitted through the reference box. The single cycle THz pulses with a temporal width of about 2 ps in time domain are transformed to the spectral pulses with a well-formed shape centered at 0.5 THz and a broad spectral width. In our experimental setup, we effectively removed multiple reflections of the THz pulses occurring from the emitter, the electro-optic crystal and a beamsplitter, which can help assure good quality of the measured time-resolved THz signals.

The thinnest sample with the thickness of 17 μm does not have the peak position of the enhanced transmission locating inside the presented spectral region. However, the two curves for the thicknesses of 75 and 153 μm in Fig. 3(a) have significant long-time oscillations with the periods of 0.87 and 1.80 picoseconds respectively, which also appears in the Fourier transformed spectra as peaks at 1.14 and 0.56 THz respectively (Fig. 3(b), gray

arrows in bottom two curves). Here the peak positions of the enhanced transmission appear at the frequency regions slightly below the Rayleigh minima $f_R = c/d$, which indicate that the transmission properties are related to the periodicity effect. On the other hand, the peak positions shift toward longer wavelength region as the sample thickness increases, keeping the typical characteristics of Fabry-Perot-like resonance. These observations indicate that the enhanced transmissions are attributed to the combined effects of the geometric shape resonance and the periodicity.

Theoretical calculations shown in Fig. 3(c) are in well agreement with the experimental results except for extremely sharp transmission peaks immediately below the first Rayleigh wavelength. In particular in the cases of the two thinnest samples, the peak linewidths have almost infinitesimal values less than several gigahertz, which cannot be experimentally observed because of the finite temporal range of time domain signals and finite sample size. Theoretically predicted peak suddenly appears at 0.56 THz for h=153 μm as shown in bottom curve of Fig. 3(b). This appearance results from the approach of the geometric shape resonance toward the first Rayleigh minimum at which the first diffracted orders become evanescent.

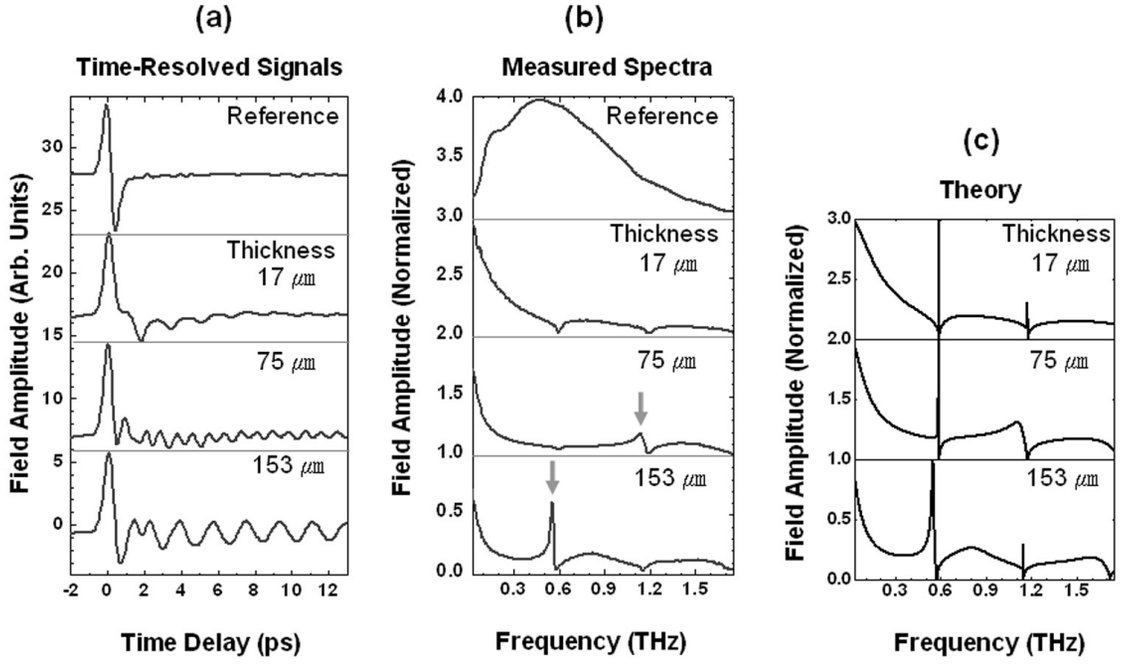

Figure 3. (a) Time traces of the incident terahertz wave (the upper figure) and the transmitted waves for three samples with a fixed period of 500 μm and different thicknesses of 17, 75, and 153 μm. The slit widths of the three samples are 78, 80, and 83 μm respectively. (b) Fourier transforms for four time traces in (a). The gray arrows represent the resonant peak positions. (c) Theoretical calculations for three samples in (b).

The independent contribution of Fabry-Perot-like resonance can draw out from single-slit approximation which can be achieved by carrying the distance between slits to be infinite. Figure 4(a) and 4(c) show the resonant peaks of transmission spectra through the samples

with the thicknesses of 75 and 153 μm respectively, theoretically predicted by the single-slit approximation. The red-shifted Fabry-Perot conditions predicted by Takakura in a single narrow slit of a thick metallic plate assure the precision of the theoretical predictions. These peak positions induced only by the Fabry-Perot-like resonance are compared with the measured angle-dependent transmission amplitudes [Fig. 4(b) and 4(d)], since the geometric shape resonance is angle-independent. For the case of the 75 μm thickness, the experimental results show a resonance band over all incident angles around 1.3 THz, which is reasonably predicted by the first Fabry-Perot-like resonance band centered at 1.2 THz [Fig. 4(a), shadowed area]. The theoretical prediction and experimental results for the sample of the 153 μm thickness also show the corresponding two spectral bands centered at 0.65 and 1.45 THz. From these theoretical prediction and experimental results, we note that the peak positions of resonant transmission can be experimentally determined by broad Fabry-Perot-like resonance band existing nearby.

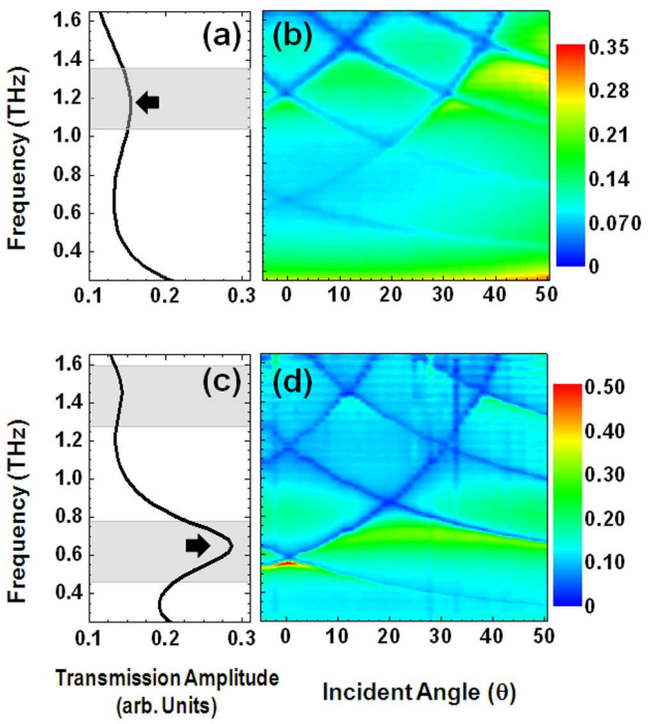

Figure 4. (a), (c) Transmission spectra, at normal incidence, predicted by single-slit approximation for the samples with the thicknesses of 75 and 153 μm respectively. Arrows represent the red-shifted first Fabry-Perot positions calculated by Takakura (Eq. (9), ref. [19]). (b), (d) Measured angle-dependent transmission spectra for the samples with the thicknesses of 75 and 153 μm respectively.

At this point, we can expect that perfect transmission phenomenon will be appeared under the condition of overlapping between the Fabry-Perot-like resonance band and totally evanescent spectral regions below the first Rayleigh wavelength. The first diffracted waves touch down on the metal surface at the wavelength of the first Rayleigh minimum, at which wavelength eventually all higher diffracted orders become evanescent which is the reason why the total incident energy can be converged to the zero-order transmission amplitude. We therefore design a thicker sample to realize the perfect transmission.

5.2. Perfect transmission in thick metallic plates

The sample with the thickness of 200 μm eventually has broad Fabry-Perot-like resonance band centered at 0.45 THz which is located in the spectral region below the first Rayleigh minimum appearing at 0.6 THz as shown in Fig. 5(a). Angle dependent transmission amplitudes [Fig. 5(b)] show the perfect transmission (in this sample, over 99% at normal incidence) centered at 0.5 THz. Despite the two transmission minima lines caused by Rayleigh frequencies for the ±1 diffraction orders, the perfect transmission appears at a broad incident angle range up to 10° because of the strong contribution of the Fabry-Perot-like resonance. Theoretical calculation with Eq. (20) is in good agreement with experimental result at normal incidence.

The perfect transmission phenomenon necessarily appears when the peak position of the enhanced transmission is located anywhere in the spectral region below the first Rayleigh frequencies, since all the diffracted orders of the transmittance T_n except for zeroth order become zero. A very useful theoretical condition for the perfect transmission can be therefore derived by setting the zeroth order reflection coefficient at zero as following

$$\left|R_0\right| = \left|1 - \frac{2iQ_0P_0}{1}\left[\frac{\cot(kh) - ikW}{1 + k^2W^2 + 2ikW\cot(kh)}\right]\right| = 0 \tag{21}$$

Below the first Rayleigh frequencies, W can be considered as

$$W = \frac{P_0Q_0}{k} + \frac{i\gamma}{k} \tag{22}$$

since all the reflected diffracted orders except for zeroth order become evanescent. Where γ is an imaginary part of kW. We can then write the condition of the perfect transmission as

$$1 - (P_0Q_0)^2 - \gamma^2 - 2\gamma\cot(kh) = 0 \tag{23}$$

For the theoretical calculation of the first Fabry-Perot-like resonance centered at 0.48 THz [Fig. 5(c)], a magnetic field profile inside the slits becomes symmetric [Fig. 5(d)] which is proved by the condition for the perfect transmission given by Eq. (23). Indeed, the magnetic field inside the slits given by Eq. (4) converges into the symmetric waveform at the first Fabry-Perot-like resonance as

$$f_2(z) \cong B\frac{\cos(kz)}{\cos(kh/2)} \tag{24}$$

since a denominator term of B is minimized under the condition of Eq. (23). It can be also intuitively understood that, under the condition of the perfect transmission at the first Fabry-Perot-like resonance, the electric field strengths at both sides of entrance and exit of the slits are the same despite opposite orientations of the electric fields at each position. Because the light coupling between resonant modes of the structured metal surfaces in the transmission and reflection regions is related to the matching condition of the phase of the

electric and the magnetic fields, the electric field strength at the entrance of the slits cannot be reproduced by the asymmetric profiles shown in Fig. 5(d).

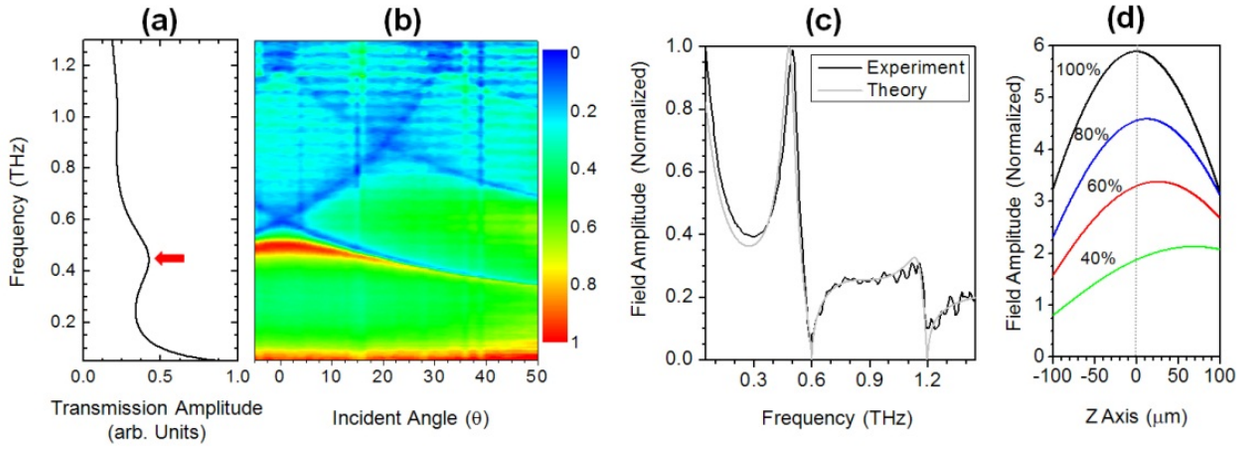

Figure 5. (a) Transmission spectra, at normal incidence, predicted by single-slit approximation for the sample with the thickness of 200 μm. An arrow represents the peak position of first Fabry-Perot-like resonance mode. (b) Measured angle-dependent transmission spectra for the sample with the thickness of 200 μm. The period is 500 μm and the slit width is 100 μm. (c) Experimental and theoretical results, at normal incidence, of the sample with the thickness of 200 μm. (d) The magnetic field profiles along the z direction inside the slits calculated by the perfect conductor model. Under the condition of the perfect transmission appearing at the first Fabry-Perot-like mode, the field profile is symmetric (black line). At neighboring frequencies with the transmission amplitudes of 80 (blue line), 60 (red line) and 40% (green line) respectively, the field profiles become asymmetric.

Near-field distributions of THz waves above the metal surfaces can also give a key for understanding the perfect transmission phenomenon. The enhancement factor of the near electric fields onto the slits can be intuitively predicted by using the language of the surface impedance as

$$Z = \frac{a}{d}\frac{E_{slit}}{H_0} + \frac{(d-a)}{d}\frac{E_{metal}}{H_0} \tag{25}$$

where E_{slit}, E_{metal} and H_0 are the electric fields along the x direction at the slits and the metal and the incident magnetic field respectively. Since the effective surface impedance becomes one under the condition of the perfect transmission and there is no tangential component of the electric field on the metal surface, we can write Eq. (25) as

$$Z_{eff} = \frac{a}{d}\frac{E_{slit}}{H_0} = 1 \tag{26}$$

The degree of the electric field enhancement is not only proportional to the incident magnetic field, but also inversely proportional to the areal sample coverage $\beta = a/d$ as

$$E_{slit} = \beta^{-1} H_0 \tag{27}$$

For the case of the areal sample coverage of $\beta = 0.2$ ($a = 100$ and $d = 500$ μm), the theoretical results show the enhancement factor of 5 on the entrance of the silts as shown in Fig. 6(a). At a specific frequency at which the perfect transmission is realized, the incident waves are focused on the entrance of the slits due to the strong evanescent waves built up by a touchdown of all orders of diffracted modes on metal surface, followed by coupled with the Fabry-Perot-like resonant modes inside the slits, and then the focused waves reached at the exit of the slits are completely converted to the transmission.

These results suggest a possibility of realizing even stronger enhancement of the electric field strength onto the slits. We therefore fabricated a sample with the areal sample coverage of $\beta = 0.1$ by increasing the period. (Reducing the slit width is actually more effective, but the technical limit of the micro-drilling method to fabricate thick metallic plates is 100 μm.) Calculated near-field distribution of the sample is given by Fig. 6(b), showing the enhancement factor of 10 corresponding to the inverse of the areal sample coverage. The near-field enhancement necessarily induces the transmission enhancement into the far-field. Measured angle dependent transmission spectra shown in Fig. 7 show not only angle-independent, broad spectral bands near 0.3 and 0.6 THz caused by the geometric shape resonance, but also a strong transmission peak with the value of about 0.85 at 0.26 THz at normal incidence. Though the peak value does not reach the THz transparency because of a narrow spectral bandwidth, the enhancement factor compared with the areal sample coverage of 0.1 is over eight. Controlling the areal sample coverage by using the period or width is therefore extremely important in realizing a high power near-field THz source.

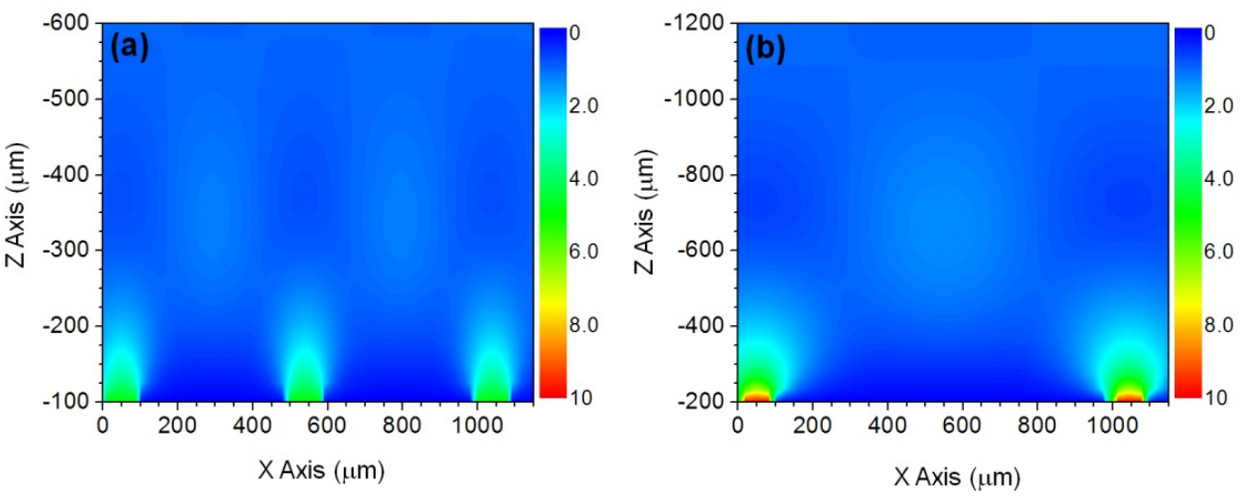

Figure 6. Electric field amplitudes for the samples with different periods of 500 (a) and 1000 μm (b) respectively. The thickness h is 400 μm and the width a is 100 μm in both cases. Enhancement factors at the entrance of the slits are 5 and 10 respectively.

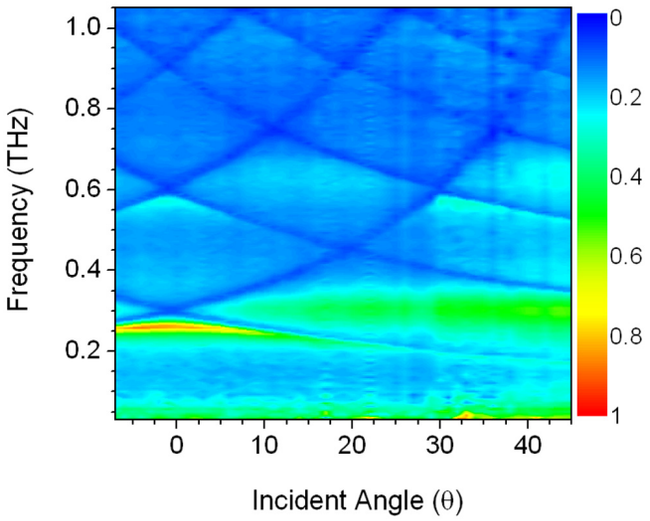

Figure 7. Measured angle-dependent transmission spectra for the sample with the period of 1000 μm. The thickness is 400 μm and the slit width is 100 μm.

5.3. THz transparency by geometric shape

At this point, it is important to understand that what the relative contributions of the periodicity and the geometric shape resonance toward the perfect transmission are in a given situation. From the experimental viewpoint, the best method to compare the difference between the relative contributions of two mechanisms is to fabricate the samples with random arrays and to investigate its transmission properties. The calculated transmission spectra as shown in Fig. 8 play an important role in determining the appropriate sample parameters. For the convenience of comparison, the transmission spectra are plotted versus the first Fabry-Perot frequency, $f_c=c/2h$ instead of the slit thickness.

In the cases of the relatively thinner metal plates, there are two peak maxima of the transmission spectra: one corresponds to the first Fabry-Perot-like mode, $f_c=c/2h$, and the other corresponds to the so-called zeroth Fabry-Perot-like mode appearing at the long wavelength region near 0 THz, which is originated from the geometric shape effect of the semi-infinite slits in a thin metal film. In the long wavelength region near 0 THz, an aluminum plate with the thickness of several hundreds of microns can be actually regarded as an optically thin metal film. With increasing the thickness of the aluminum plates, the peak maxima originating from higher Fabry-Perot-like modes such as $f_c=2c/2h$, $3c/2h$, and etc are added consecutively, maintaining the perfect transmission.

All curves of the Fabry-Perot-like modes show that the curves approach to straight lines of the classical Fabry-Perot positions (Fig. 8, dotted lines) as getting away from the wavelength of the first Rayleigh minimum of 0.6 THz. The calculated results may therefore present that, when the peak maxima approach to the long wavelength limit, the contribution by the coupled evanescent surface modes presented in Eq. (19) becomes weak. In our experiments, we therefore fabricated the samples of periodic and random arrays of slits with the thickness of 400 μm since in which there are three different peak maxima originating from the zeroth

(Fig. 8, C), first (Fig. 8, B) and second (Fig. 8, A) Fabry-Perot-like modes and each peak maximum may be stimulated by different contributions of the periodicity and the geometric shape. In fact, as the peak position is getting away from the wavelength of the first Rayleigh minimum toward longer wavelength region, the geometric shape effect becomes dominant.

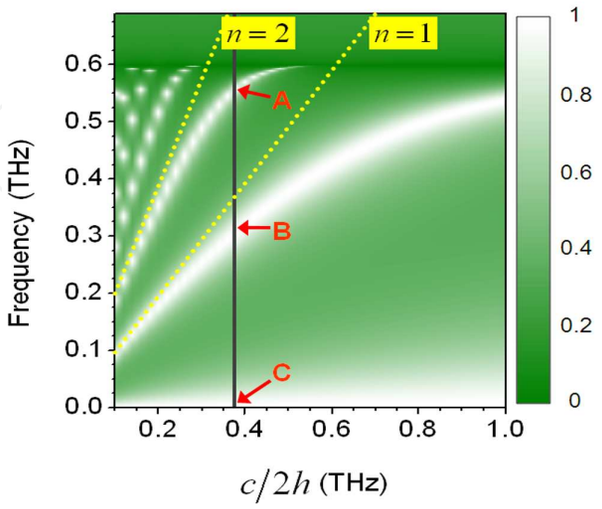

Figure 8. Calculated transmission spectra plotted versus the frequency of the first Fabry-Perot-like resonance. The dotted lines represent the first and second classical Fabry-Perot resonances. The sample with the thickness of 400 μm has three Fabry-Perot resonance modes (A, B, and C) appearing at the frequency region below the first Rayleigh minimum.

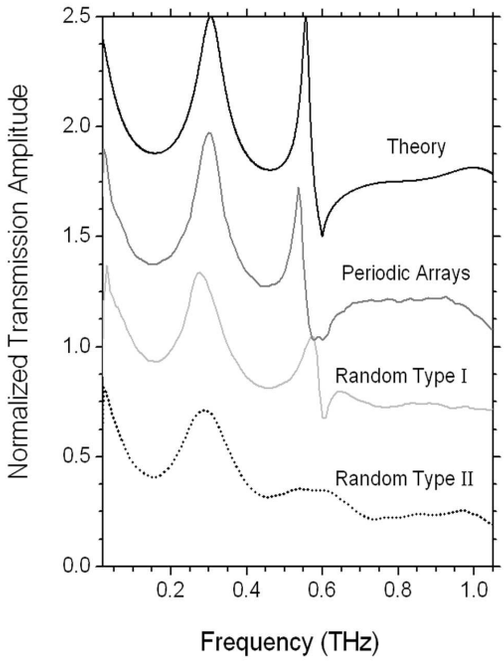

Figure 9. Normalized transmission spectra at normal incidence for three types of the samples: periodic arrays (dark gray line), random type I (bright gray line), and random type II (dotted line). The black line is the calculated transmission spectra for the case of the periodic arrays. These samples have same areal sample coverage of 0.2 and same thickness of 400 μm. The randomization of the slit structures is based on the different frozen-phonon fashion.

Figure 9 shows the normalized transmission amplitudes of periodic and random arrays of silts at normal incidence. Here the samples have same slit width a of about 100 μm and same areal sample coverage of β=0.2. As predicted in theoretical calculations, the calculated transmission spectrum (Fig. 9, a solid line) shows three peak maxima at 0.56, 0.30 and near zero THz, corresponding to the second, first and zeroth Fabry-Perot-like modes respectively. The measured transmission spectrum (Fig. 9, a dark gray line) of the periodic arrays of slits agrees well with the calculated one, except slight disagreement at the peak maximum of the second Fabry-Perot-like mode. Here the experimental linewidth of the second Fabry-Perot-like mode does not completely reproduce the theoretical one since which is too sharp to experimentally observe in real sample.

We then consider two random structures with the different frozen-phonon fashion of neighboring slits. The Random Type I and II samples were fabricated by displacing the position of each slit of periodic arrays with random amounts of ± $d/4$ and ± $d/2$ respectively. The transmission spectrum of the Random Type I (Fig. 9, a bright gray line) shows a slightly lower peak value at 0.30 THz and a considerably decreased peak value at 0.56 THz, but overall the spectral shape of the transmission spectra are well matched, particularly reproducing the peak value due to the zeroth Fabry-Perot-like mode. The measured transmission spectrum of the Random Type II (Fig. 9, a dotted line) clearly exhibits the spectral properties of the perfectly random arrays of slits, which does not show any more the transmission minimum at 0.6 THz originating from the first Rayleigh minimum due to the periodicity effect only. On the other hand, although the peak value appearing near 0.3 THz is slightly decreased with further increasing the fraction of random amounts, the spectral shape and peak position can be not only considered unchangeable, the resonant peak also exhibits an enhancement factor larger than 3.5. Furthermore, the resonant peaks of the zeroth Fabry-Perot-like mode are more dramatic where all the transmission spectra in theory and experiments are perfectly matched, showing the transmittance more than 80%.

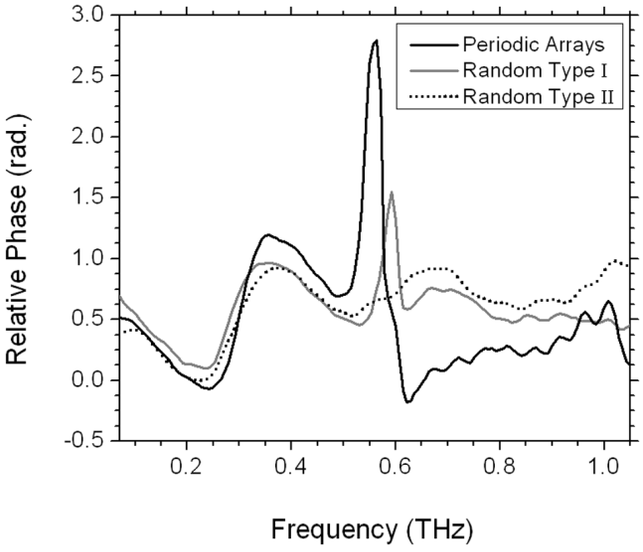

Figure 10. Relative phase changes in radians at normal incidence for three types of the samples: periodic arrays (black line), random type I (gray line), and random type II (dotted line).

The relative phase of transmitted THz waveforms not only improves the understanding for the relative contributions of the geometric shape and the periodicity but also makes more clearly what the dominant mechanism in enhancing the THz transmission is. When the geometric shape effect becomes dominant, there will be a little difference between the random and periodic arrays of slits, as shown in Fig. 10. In addition, the geometric shape does not depend on the incident angle of the THz waves. Shown in Fig. 11 are the angle dependent transmission amplitudes for the samples. For the sample of periodic arrays of slits, there are two dominant transmission minima lines crossing at 0.6 THz at zero angle which is the Rayleigh wavelengths corresponding to the ±1 diffracted orders as

$$f_{\pm 1}(\theta) = \frac{c}{d[1 \mp \sin(\theta)]} \tag{28}$$

The Rayleigh wavelengths determined by the grating period distinctly appear as transmission minima lines over all the incident angle of the THz waves, generating an angle-dependent and strongly enhanced transmission peak near 5.4 THz. With increasing the randomness, the transmission minima lines of the Rayleigh wavelengths become indistinct as shown in Fig. 11(b) and eventually disappear as shown in Fig. 11(c). Similarly, the angle dependent transmission peak appearing at the sample of periodic arrays of slits also disappears since its strong enhancement is caused by the strong field accumulation of the evanescent surface waves by the periodic structures. On the contrary, the enhanced peaks appearing near 0.3 THz are essentially angle independent, making the strong enhancement.

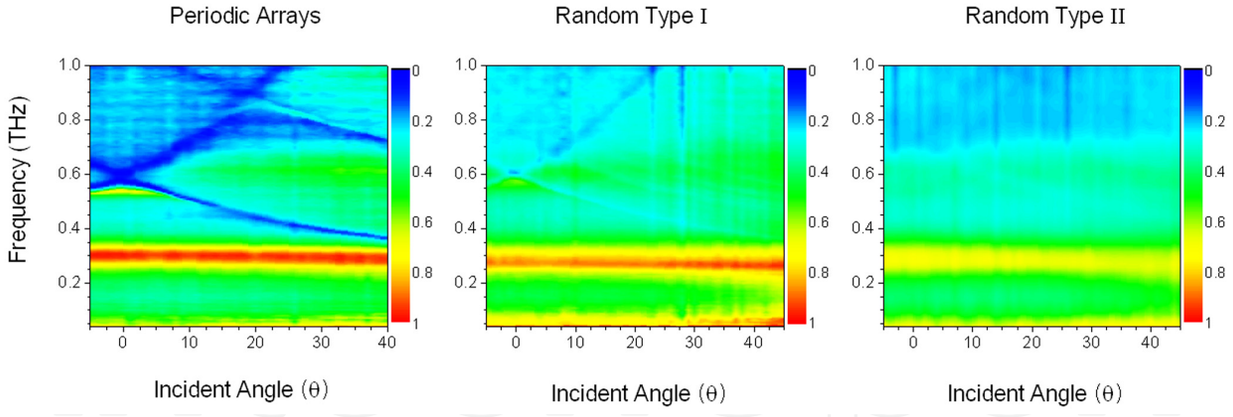

Figure 11. Normalized angle dependent transmission amplitudes for three types of the samples: periodic arrays (a), random type I (b), and random type II (c).

6. Conclusion

In conclusion, we have demonstrated two mechanisms for perfect transmission appearing at specific frequencies through the periodic and random arrays of slits. The theoretical results show that the perfect transmission can be realized in spectral region below the first Rayleigh minimum determined by the periodicity. Under the condition for the perfect transmission, the symmetric electric- and magnetic-field profiles inside the slits are excited and the

incident energy is funneled onto the slits with the enhancement factor proportional to the inverse of the areal sample coverage. The measured transmission spectra through the slits of thick metal plates show the enhanced transmission of perfect transmission, which is attributed by the increase of the spectral linewidth resulting from the approach of the geometric shape resonance to the spectral region below the first Rayleigh minimum. The resonant bands of the geometric shape presented by the single silt approximation and the measured angle dependent transmission spectra not only are angle independent but also determine the spectral peak positions of the perfect transmission.

The random arrays of slits designed to remove the effect of the periodicity clearly show the dominant contribution of the geometric shape resonance toward the enhanced transmission. In the long-wavelength region far from the first Rayleigh minimum, the geometric shape resonance becomes dominant and the transmission enhancement factors are almost equal to the cases of the periodic arrays of slits. The strong transmission and local field enhancements open a possibility of potential applications in perfect transmission of solid materials such as semiconductors and biological materials requiring the high power THz sources and in designing photonic devices such as transmission filters, low-pass frequency filters, and transmissive waveguides requiring high transmission at desired frequencies.

Author details

Joong Wook Lee*
Advanced Photonics Research Institute, GIST, Gwangju, Republic of Korea

DaiSik Kim
Department of Physics and Astronomy, Seoul National University, Seoul, Republic of Korea

Acknowledgement

The authors gratefully thank Q. H. Park and M. A. Seo for useful discussions and S. C. Jeoung for sample preparation. This research was supported by Basic Science Research Program through the National Research Foundation of Korea (NRF) funded by the Ministry of Education, Science and Technology (2010-0021181) and by the APRI Research Program of GIST.

7. References

[1] Ebbesen T. W., Lezec H. L., Ghaemi H. F., Thio T., and Wolff P. A. (1998) Extraordinary optical transmission through sub-wavelength hole arrays. Nature 391: 391, 667-669.
[2] Wood R. W. (1902) On a remarkable case of uneven distribution of light in a diffraction grating spectrum. Phil. Mag. 4: 396-408.
[3] Rayleigh L. (1907) On the passage of electric waves through tubes, or the vibrations of dielectric cylinders. Phil. Mag. 14: 60-65.

* Corresponding Author

[4] Fano U. (1941) The theory of anomalous diffraction gratings and of quasi-stationary waves on metallic surfaces (Sommerfeld's waves). J. Opt. Soc. Am. 31: 213-222.
[5] Hessel A. and Oliner A. A. (1965) A New Theory of Wood's Anomalies on Optical Gratings. Appl. Opt. 4: 1275-1297.
[6] Ulrich R. (1968) Interference filters for the far infrared. Appl. Opt. 7: 1987-1996.
[7] Chen C. C. (1970) Transmission Through a Conducting Screen Perforated Periodically with Apertures. IEEE trans. Microwave Theory Tech. 18: 627-632.
[8] Bliek P. J., Botten L. C., Deleuil R., Paedran R. C. M., and Maystre D. (1980) Inductive grids in the region of diffraction anomalies: theory, experiment, and applications. IEEE trans. Microwave Theory Tech. 28: 1119-1125.
[9] Keilmann F. (1981) Infrared high-pass filter with high contrast. Int. J. Infrared Millimeter Waves 2: 259-272.
[10] Ulrich R. (1974) Modes of propagation on an open periodic waveguide for the far-infrared, in optical and acoustical micro-electronics, ed. by J. Fox, Micr. Res. Inst. Symp. Series 23: Polytec. Press, New York 359-376.
[11] Lochbihler H. and Depine R. (1993) Highly conducting wire gratings in the resonance region. Appl. Opt. 32: 3459-3465.
[12] Lochbihler H. (1994). Surface polaritons on gold-wire gratings. Phys. Rev. B 50: 4795-4801.
[13] Porto J. A., Garcia-Vidal F. J., and Pendry J. B. (1999) Transmission resonances on metallic gratings with very narrow slits. Phys. Rev. Lett. 83: 2845-2848.
[14] Cao Q. and Lalanne P. (2002) Negative role of surface plasmons in the transmission of metallic gratings with very narrow slits. Phys. Rev. Lett. 88: 057403.
[15] Collin S., Pardo F., Teissier R., and Pelouard J. L. (2002) Horizontal and vertical surface resonances in transmission metallic gratings. J. Opt. A: Pure Appl. Opt. 4: 154-160.
[16] Astilean S., Lalanne P., and Palamaru M. (2000) Light transmission through metallic channels much smaller than the wavelength. Opt. Commun.175: 265-273.
[17] Treacy M. M. J. (1999) Dynamical diffraction in metallic optical gratings. Appl. Phys. Lett. 75: 606-608.
[18] Lee K. G. and Park Q. H. (2005) Coupling of Surface Plasmon Polaritons and Light in Metallic Nanoslits. Phys. Rev. Lett. 95: 103902.
[19] Takakura Y. (2001) Optical resonance in a narrow slit in a thick metallic screen. Phys. Rev. Lett. 86: 5601-5603.
[20] Yang F. and Sambles J. R. (2002) Resonant Transmission of Microwaves through a Narrow Metallic Slit. Phys. Rev. Lett. 89: 063901.
[21] Martin-Moreno L., Garcia-Vidal F. J., Lezec H. J., Pellerin K. M., Thio T., Pendry J. B., and Ebbesen T. W. (2001) Theory of extraordinary optical transmission through subwavelength hole arrays. Phys. Rev. Lett. 86: 1114-1117.
[22] Salomon L., Grillot F., Zayats A. V., and Fornel F. (2001) Near-field distribution of optical transmission of periodic subwavelength holes in a metal film. Phys. Rev. Lett. 86: 1110-1113.
[23] Martin-Moreno L. and Garcia-Vidal F. J. (2004) Optical transmission through circular hole arrays in optically thick metal films. Opt. Express 12: 3619-3628.

[24] Hohng S. C., Yoon Y. C., Kim D. S., Malyarchuk V., Muller R., Lienau C., Park J. W., Yoo K. H., Kim J., Ryu H. Y., and Park Q. H. (2002) Light emission from the shadows: Surface plasmon nano-optics at near and far fields. Appl. Phys. Lett. 81: 3239-3242.
[25] Kim D. S., Hohng S. C., Malyarchuk V., Yoon Y. C., Ahn Y. H., Yee K. J., Park J. W., Kim J., Park Q. H., and Lienau C. (2003) Microscopic Origin of Surface-Plasmon Radiation in Plasmonic Band-Gap Nanostructures. Phys. Rev. Lett. 91: 143901.
[26] Ropers C., Park D. J., Stibenz G., Steinmeyer G., Kim J., Kim D. S., and Lienau C. (2005) Femtosecond light transmission and subradiant damping in plasmonic crystals. Phys. Rev. Lett. 94: 113901.
[27] Gordon R. and Brolo A. G. (2005) Increased cut-off wavelength for a subwavelength hole in a real metal. Opt. Express 13: 1933-1938.
[28] Klein Koerkamp K. Enoch J., S., Segerink F. B., Van Hulst N. F., and Kuipers L. (2004) Strong influence of hole shape on extraordinary transmission through periodic arrays of subwavelength holes. Phys. Rev. Lett. 92: 183901.
[29] Degiron A. and Ebbesen T. W. (2005) The role of localized surface plasmon modes in the enhanced transmission of periodic subwavelength apertures. J. Opt. A: Pure Appl. Opt. 7: S90-S96.
[30] van der Molen K. L., Klein Koerkamp K. J., Enoch S., Segerink F. B., Van Hulst N. F., and Kuipers L. (2005) Role of shape and localized resonances in extraordinary transmission through periodic arrays of subwavelength holes: Experiment and theory. Phys. Rev. B 72: 045421.
[31] Ruan Z. and Qiu M. (2006) Ehanced transmission through periodic arrays of subwavelength holes: the role of localized waveguide resonances. Phys. Rev. Lett. 96: 233901.
[32] Lee J. W., Seo M. A., Kang D. H., Khim K. S., Jeoung S. C., and Kim D. S. (2007) Terahertz electromagnetic wave transmission through single rectangular holes and slits in thin metallic sheets. Phys. Rev. Lett. 99: 137401.
[33] Bethe H. A. (1944) Theory of diffraction by small holes. Phys. Rev. 66: 163-182.
[34] Boukamp C. J. (1954) Diffraction Theory. Rep. Prog. Phys. 17 : 35-100.
[35] García de Abajo F. J. (2002) Light transmission through a single cylindrical hole in a metallic film. Opt. Express 10: 1475-1484.
[36] Degiron A., Lezec H. J., Yamamoto N., and Ebbesen T. W. (2004) Optical transmission properties of a single subwavelength aperture in a real metal. Opt. Commun. 239: 61-66.
[37] Garcia-Vidal F. J., Moreno E., Porto J. A., and Martin-Moreno L. (2005) Transmission of light through a single rectangular hole. Phys. Rev. Lett. 95: 103901.
[38] Van Exter M. and Grischkowsky D. (1990) Optical and electronic properties of doped silicon from 0.1 to 2 THz. Appl. Phys. Lett. 56: 1694-1696.
[39] Jiang Z., Li M., and Zhang X. C. (2000) Dielectric constant measurement of thin films by differential time-domain spectroscopy. Appl. Phys. Lett. 76: 3221-3223.
[40] Kang C., Maeng I. H., Oh S. J., Son J. H., Jeon T. I., An K. H., Lim S. C., and Lee Y. H. (2005) Frequency-dependent optical constants and conductivities of hydrogenfunctionalized single-walled carbon nanotubes. Appl. Phys. Lett. 87: 041908.

[41] Han H., Park H., Cho M., and Kim J. (2002) THz pulse propagation in plastic photonic crystal fiber. Appl. Phys. Lett. 80: 2634-2636.
[42] Hara J. F., Averitt R. D., and Taylor A. J. (2004) Terahertz surface plasmon polariton coupling on metallic gratings. Opt. Express 12: 6397-6402.
[43] Torosyan G., Rau C., Pradarutti B., and Beigang R. (2004) Generation and propagation of surface plasmons in periodic metallic structures. Appl. Phys. Lett. 85: 3372-3374.
[44] Gomez Rivas J., Schotsch C., Haring Bolivar P., and Kurz H. (2003) Enhanced transmission of THz through subwavelength holes. Phys. Rev. B 68: 201306.
[45] Gomez Rivas J., Kuttge M., Haring Bolivar P., and Kurz H. (2004) Propagation of surface plasmon polaritons on semiconductor gratings. Phys. Rev. Lett. 93: 256804.
[46] Lee J. W., Seo M. A., Kim D. S., Jeoung S. C., Lienau Ch., Kang J. H. and Park Q. H. (2006) Fabry-Perot effects in THz time-domain spectroscopy of plasmonic band-gap structures. Appl. Phys. Lett. 88: 071114.
[47] Azad A. K., Zhao Y., and Zhang W. (2005) Transmission properties of terahertz pulses through an ultrathin subwavelength silicon hole array. Appl. Phys. Lett. 86: 141102.
[48] Qu D., Grischkowsky D., and Zhang W. (2004) Terahertz transmission properties of thin, subwavelength metallic hole arrays. Opt. Lett. 29: 896-898.
[49] Cao H. and Nahata A. (2004) Influence of aperture shape on the transmission properties of a periodic array of subwavelength apertures. Opt. Express 12: 3664-3672.
[50] Shin Y. M., So J. K., Jang K. H., Won J. H., Srivastava A., and Park G. S. (2007) Superradiant terahertz smith-purcell radiation from surface-plasmon excited by counter-streaming electron beams. Appl. Phys. Lett. 90: 031502.
[51] Jeon T. I., Zhang J., and Grischkowsky D. (2005) THz Sommerfeld wave on a single metal wire. Appl. Phys. Lett. 86: 161904.
[52] Jeon T. I. and Grischkowsky D. (2006) THz Zenneck surface wave propagation on a metal sheet. Appl. Phys. Lett. 88: 061113.
[53] Seo M. A., Park H. R., Koo S. M., Park D. J., Kang J. H., Suwal O. K., Choi S. S., Planken P. C. M., Park G. S., Park N. K., Park Q. H. and Kim D. S. (2009) Terahertz field enhancement by a metallic nano slit operating beyond the skin-depth limit. Nature Pnoton. 3: 152-156.
[54] Matsui T., Agrawal A., Nahata A. and Vardeny Z. V. (2007) Transmission resonances through aperiodic arrays of subwavelength apertures. Nature 446: 517-521.
[55] Williams C. R., Andrews S. R., Maier S. A. Fernández-Domínguez A. I., Martín-Moreno L., and García-Vidal F. J. (2007) Highly confined guiding of terahertz surface plasmon polaritons on structured metal surfaces. Nature Photon 2: 175-179.
[56] Pendry J. B., Martin-Moreno L., and Garcia-Vidal F. J. (2004) Mimicking Surface Plasmons with Structured Surfaces. Science 305: 847-848.
[57] Garcia-Vidal F. J., Martin-Moreno L., and Pendry J. B. (2005) Surfaces with holes in them: new plasmonic metamaterials. J. Opt. A: Pure Appl. Opt. 7: S97-S101.
[58] Hibbins A. P., Evans B. R., and Sambles J. R. (2005) Experimental verification of designer surface plasmons. Science 308: 670-672.

[59] Garica de Abajo F. J., Gomez-Santos G., Blanco L. A., Borisov A. G., and Shabanov S. V. (2005) Tunneling mechanism of light transmission through metallic films. Phys. Rev. Lett. 95: 067403.

[60] Garcia de Abajo F. J., Gomez-Medina R., and Saenz J. J. (2005) Full transmission through perfect-conductor subwavelength hole arrays. Phys. Rev. E 72: 016608.

[61] Treacy M. M. J. (2002) Dynamical diffraction explanation of the anomalous transmission of light through mettallic gratings. Phys. Rev. B 66: 195105.

[62] Garcia-Vidal F. J. and Martin-Moreno L. (2002) Transmission and focusing of light in one-dimensional periodically nanostructured metals. Phys. Rev. B 66: 155412.

[63] Kang J. H., Park Q. H., Lee J. W., Seo M. A., and Kim D. S. (2006) Perfect transmission of THz waves in structured metals. J. Korean Phys. Soc. 49: 881-884.

[64] Lee J. W., Seo M. A., Park D. J., Jeoung S. C., Park Q. H., Lienau Ch., and Kim D. S. (2006) Terahertz transparency at Fabry-Perot resonances of periodic slit arrays in a metal plate: experiment and theory. Opt. Express 14: 12637-12643.

[65] Tanaka M., Miyamaru F., Hangyo M., Tanaka T., Akazawa M., and Sano E. (2005) Effect of a thin dielectric layer on terahertz transmission characteristics for metal hole arrays. Opt. Lett. 30: 1210-1212.

[66] Lee J. W., Seo M. A., Park D. J., Kim D. S., Jeoung S. C., Lienau Ch., Park Q-Han, and Planken P. C. M. (2006) Shape resonance omni-directional terahertz filters with near-unity transmittance. Opt. Express 14: 1253-1259.

[67] Lee J. W., Seo M. A., Sohn J. Y., Ahn Y. H., Kim D. S., Jeoung S. C., Lienau Ch., and Park Q-Han (2005) Invisible plasmonic metamaterials through impedance matching to vacuum. Opt. Express 13: 10681-10687.

[68] Zhao G., Schouten R. N., Van der Valk N., Wenckebach W. Th., and Planken P. C. M. (2002) Design and performance of a THz emission and detection setup based on a semi-insulating GaAs emitter. Rev. Sci. Instrum. 73: 1715-1719.

[69] Saleh B. E. A. and Teich M. C. (1991) Fundamentals of Photonics. John Wiley & Sons, Inc.

[70] Wu Q. and Zhang X. C. (1995) Free-space electro-optic sampling of terahertz beams. Appl. Phys. Lett. 67: 3523-3525.

[71] Lee J. W. and Kim D. S. (2009) Relative contribution of geometric shape and periodicity to resonant terahertz transmission. J. Appl. Phys. 107: 113109.

[72] Nau D., Schönhardt A., Bauer Ch., Christ A. I., Zentgraf T., Kuhl J., Klein M. W., and Giessen H. (2007) Correlation effects in disordered metallic photonic crystal slabs. Phys. Rev. Lett. 98: 133902.